Synthesis and Characterization of Nanostructured Zno Dilute Magnetic Semiconductor: Insight of the Role of Mg and Mn-Impurity

Hazem Bouraoui[1,2*], Soufiane Benhamida[3], Yamina Benkrima[4]

[1]Univ. Ouargla, Fac. des Mathématiques et Sciences de la Matière, route de Ghardaia, Ouargla 30000, Algeria.

[2]Laboratoire de Cristallographie, Université Mentouri, Constantine, Algérie.

[3]Laboratoire de Rayonnement et Plasmas et Physique des Surfaces (LRPPS), Faculté des Mathématiques et des Sciences de la Matière, Université Kasdi Merbah Ouargla, Ouargla 30000, Algeria.

[4]Ecole Normale Superieure de Ouargla 30000, Algeria.

Email: bouraoui-hazem@univ-ouargla.dz

Received 22 /09/ 2022; Accepted 23/12/ 2022, Published 07/01/2023

Abstract

This study employed the nebulizer spray pyrolysis (NSP) technique to synthesize pure ZnO, Mg-doped ZnO, and Mn-doped ZnO nanostructured thin layers at 400°C on a glass substrate. The impact of Mg^{2+} and Mn^{2+} ion doping concentration on ZnO's microstructural optical and magnetic properties was studied. X-ray diffraction results showed the formation of polycrystalline ZnO with hexagonal wurtzite structure and (002) plane as the preferred orientation. The crystallite size has decreased from 29.899 nm to 20.891 nm with the addition of Mg^{2+} and Mn^{2+} ions. Raman spectra show that the intensity of vibrational modes increased with the effect of doping. All prepared thin layers exhibited high transmission, around 85% in visible regions. The band gap energy increases slightly from 3.28 to 3.31 eV. Hysteresis loop confirms the ferromagnetic properties of the samples.

Keywords: nebulizer spray pyrolysis (NSP), ZnO thin layers, XRD, Optical properties; magnetic properties.

Tob Regul Sci.™ 2023;9(1): 6474 - 6482

DOI: doi.org/10.18001/TRS.9.1.453

introduction:

Nanotechnology involves manipulating matter's physical and chemical properties at the nanometer scale to create and use materials, devices, and systems. It has the potential to completely transform the methods of creating materials and appliances and expand the variety and capabilities that may be achieved [1]. Recently, significant attention has been paid to diluted magnetic semiconductors (DMS) in magnetic semiconductor research. DMS refers to normal semiconductors where many atoms are replaced by elements that generate localized magnetic

moments inside the semiconductor matrix [2]. Zinc oxide (ZnO) has a wide optical band gap of approximately 3.4 eV. It has garnered significant interest because of its impressive physical and chemical properties and large excitonic binding energy of around 60 meV. ZnO is an ideal selection as a host material for magnetic semiconductors due to its cost-effectiveness, abundance in nature, nontoxicity, and chemical inertness [3-5]. ZnO is employed in diluted magnetic semiconductors, smart windows, digital displays, and other related technologies. An important factor in enhancing and optimizing the characteristics of ZnO is the introduction of dopant ions into the ZnO host lattice. Utilizing chosen elements for doping provides a highly effective approach to augmenting and regulating the structural, electrical, optical, and magnetic characteristics of ZnO materials [6]. Many reports have investigated using ZnO doped with elements like Mg, Mn, Ni, Fe, and Cd for practical purposes, demonstrating that these elements exhibit a consistently stable ferromagnetic property [7-11]. ZnO thin layers can be synthesized using various manufacturing techniques, such as thermal decomposition, chemical vapor deposition, co-precipitation, nebulizer spray pyrolysis, hydrothermal, etc. [12-16]. Among the several methods available, nebulizer spray pyrolysis is a highly appealing choice for synthesizing ZnO thin films and achieving large-scale production [6]. In the present paper, pure ZnO, Mg-doped ZnO, and Mn-doped ZnO nanostructured thin layers have been synthesized via the nebulizer spray pyrolysis (NSP) method on a glass substrate. The impact of Mg^{2+} and Mn^{2+} ion doping concentration on the microstructural optical and magnetic properties of ZnO was investigated in this study.

2. Materials and preparation

pure ZnO, Mg-doped ZnO, and Mn-doped ZnO nanostructured thin layers were fabricated successfully on ordinary glass substrates via the nebulizer spray pyrolysis (NSP) technique. Zinc(II) acetate dehydrate [$Zn(CH_3COO)_2.2H_2O$] was used as the source of Zn, Magnesium(II) dichloride hexahydrate ($MgCl_2.6H_2O$) and Manganese (II) chloride tetrahydrate ($MnCl_2.4H_2O$) were the source of Mg and Mn, respectively. At first, an appropriate amount of zinc acetate dehydrate was dissolved in 30 ml of distilled water to get the molar concentration of 0.1 mol/l. The mixture solution was magnetically stirred at 50 °C for 30 min to obtain a clear, homogeneous solution. Doping samples were obtained by adding (5%wt) of $MgCl_2.6H_2O$ and $MnCl_2.4H_2O$ separately to the previous solution. The obtained mixture solution was sprayed onto a cleaned glass substrate via nebulizer spray pyrolysis (NSP), where the substrate temperature was fixed at 400 °C using a temperature controller, and the distance between the atomizer and substrate was equal to 15 cm. Finally, all prepared samples were allowed to cool in an atmosphere of air after the deposition process.

3. Characterization methods

Microstructural properties of all prepared films were investigated using a Bruker D8 Advance diffractometer with CuKα radiation (λ= 1.540593Å) in the 2θ range from 20° to 60°. Raman scattering measurements were studied using the Lab RAM HR Evolution system (Horiba Jobin-Yvon) coupled with a He–Cd laser excitation at 425 nm. All synthesized films' optical properties were characterized using a Cray 100 Agilent UV–Vis–NIR spectrophotometer recorded at a

wavelength ranging from 300 to 900 nm. At room temperature, the Microsenise EZ9 Vibrating Sample Magnetometer (VSM) determined the magnetic properties.

4. Results and discussion

4.1. Structural properties

Fig. 1 shows the X-ray diffraction patterns of pure ZnO, Mg-doped ZnO, and Mn-doped ZnO thin layers. Through the XRD analysis, it can be observing the presence of defined diffraction peaks along 2θ = 34.64°, 36.30°, and 47.68° which are associated respectively to (002), (101), and (102) planes of hexagonal wurtzite ZnO structure with space group P63mc (186) according to ICDD (00-001-1136) card [17]. Furthermore, it can be seen that all samples are polycrystalline in nature, with a high intense (002) diffraction peak detected in all deposited films, indicating a predominant orientation of the ZnO crystallites along the c-axis. It also shows that this plane's intensity increases in the case of Mg-doped ZnO and Mn-doped samples, which can be interpreted as the improved crystallinity of the ZnO films. No characteristic peaks corresponding to Mg and Mn or their oxides appear in the XRD results, indicating that Mg^{2+} and Mn^{2+} ions are incorporated well at the Zn lattice sites.

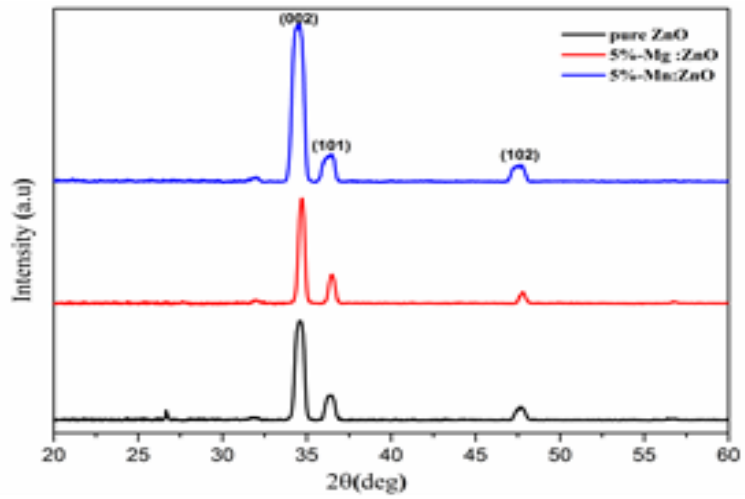

Fig. 1. X-ray diffraction pattern of pure ZnO, Mg-doped ZnO, and Mn-doped ZnO thin films.

The average crystallite size (D) of our thin films was calculated using Scherrer's equation for the most intense peak (002) using the following formula [18]:

$$D = \frac{k\lambda}{\beta \cos\theta} \quad (1)$$

Where D is the average crystallite size, k =0.89 is the coefficient, • is the full width at half maximum (FWHM), λ is the wavelength of X-rays (Cu-Ka= 0.154 nm), and θ is the Bragg diffraction angle. The c-axis lengths were estimated from the most intense peak at the (002) plane, using the formula below [19]:

$$c = \frac{\lambda}{sin\theta} \quad (2)$$

The formula evaluated the strain of the film (ε) [20]:

The calculated values of structural parameters such as c-axis lengths (c), average crystallite size (D), and micro-strain (ε) for all samples are summarized in Table 1.

Table 1. Values of Bragg angle 2θ, c-axis length, crystallite size D, and micro-strain ε for the (200) plane of pure ZnO, Mg-doped ZnO, and Mn-doped ZnO thin films.

Samples	2θ (deg)	*c-axis length* (Å)	Crystallite size *D* (*nm*)	*Micro-strain* (ε)$\times 10^{-4}$
Pure ZnO	34,346	5,220	26,123	13,12
(5%) Mg-doped ZnO	34,838	5,148	29,899	11,46
(5%) Mn-doped ZnO	34,192	5,243	20,891	16,40

It is observed from Table 1. that the lattice parameter c-axis length is decreased from 5.220(Å) to 5.148 (Å) in the Mg-doped ZnO sample; this may be due to the incorporation of Mg ions in the ZnO lattice structure because the Mg^{+2} ionic radii (= 0.66Å) being smaller compared to Zn^{+2} (= 0.74 Å) [6]. Whereas a slight increase rich 5.243 (Å) in lattice parameter c from Mn-doped ZnO sample, these expansions confirm the existence of the Mn ion in the ZnO host structure. On the other hand, the estimated crystallite sizes (D) are about 26.123 nm, 29.899 nm, and 20.891 nm through pure ZnO, Mg-doped ZnO, and Mn-doped ZnO films, respectively. These changes in D values indicate that the addition of manganese or magnesium ions occupying Zn sites and the results in the crystallization and crystallite growth were changed along the c-axis of the ZnO crystal structure [6].

4.2. Raman spectrum studies

Fig. 2 displays room temperature Raman spectra of the synthesized samples, recorded from 400 cm^{-1} to 900 cm^{-1}. It can be seen from Fig. 2 the existence of characteristic peaks at about 435, 567and 789 cm^{-1}; these peaks correspond respectively to E2 polar mode, the optical longitudinal (OL) E1 mode, and A1(LA+TO) vibration mode. All detected peaks are linked to the bulk ZnO wurtzite structure [21]. We can observe that the intensity related to the E2 polar mode and

optical longitudinal (OL) E1 in doped samples increased significantly; these results can be attributed to the substitution of Mg^{2+} or Mn^{2+} ions on the Zn^{+2} sites of zinc oxide crystal [22].

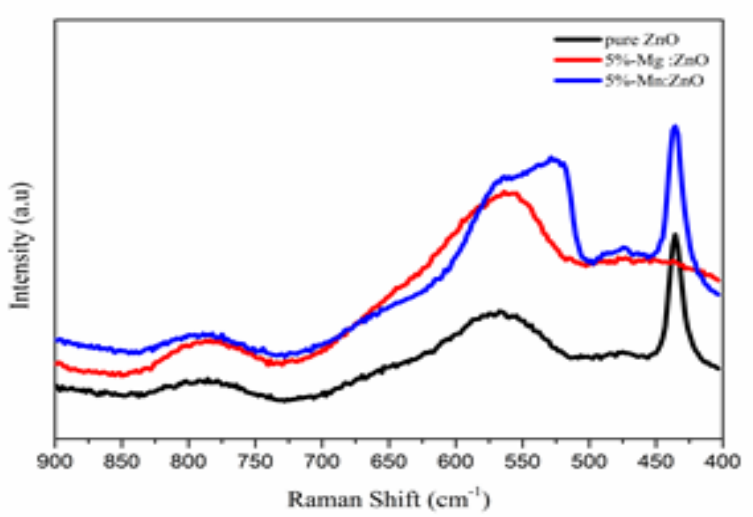

Fig. 4. Raman spectra of pure ZnO, Mg-doped ZnO, and Mn-doped ZnO thin films.

4.3. Optical properties

The optical transmittance spectra of pure ZnO, Mg-doped ZnO, and Mn-doped ZnO thin layers measured in the range of 300–900 nm are shown in Fig.3. It is seen from Fig.3 that all prepared films exhibit high transparency in the visible region. In contrast, the average transmission values varied from 62% to 85%. We can see that the pure ZnO showed a maximum transmittance of around 85%, while a decrease in transmission is observed in Mg and Mn-doped ZnO samples. The decrease in transmittances may be due to the increase in film thickness, which leads to an increase in the scattering of photons by the surface roughness of the films. A sharp absorption between 350-365 nm in the UV region reveals the onset fundamental absorption edge [21].

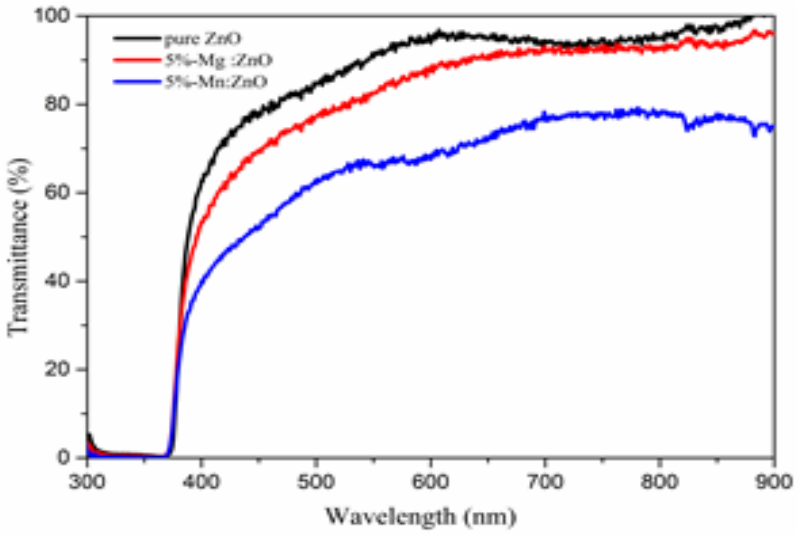

Fig. 3. Transmittance spectra of pure ZnO, Mg-doped ZnO, and Mn-doped ZnO thin films.

In order to estimate the values of energy bandgap (Eg) in all prepared samples in the case of direct allowed transitions, we can use the Tauc law expressed by [18]:

$$(\alpha h\nu) = C(h\nu - E_g)^{\frac{1}{2}} \quad (3)$$

Where α is the absorption coefficient, C is the constant, h is the planks constant, ν is the photon energy, and Eg is the energy band gap. The Eg values can obtained by plotting (αhν)2 as a function of (hν) and drawing the straight line portion of the plot to the (hν) axis, as displayed in Fig.4. The Eg values were found to be 3.28, 3.29 and 3.31 eV for pure ZnO, Mg-doped ZnO and Mn-doped ZnO thin layers, respectively. It was seen that the Eg values increase gradually with the addition of Mg^{2+} and Mn^{2+} ions compared with pure ZnO film. This increase is attributed to the Burstein-Moss effect, where introducing new elements in the ZnO lattice creates new defects due to the difference in their electronegativity and ion radii [23].

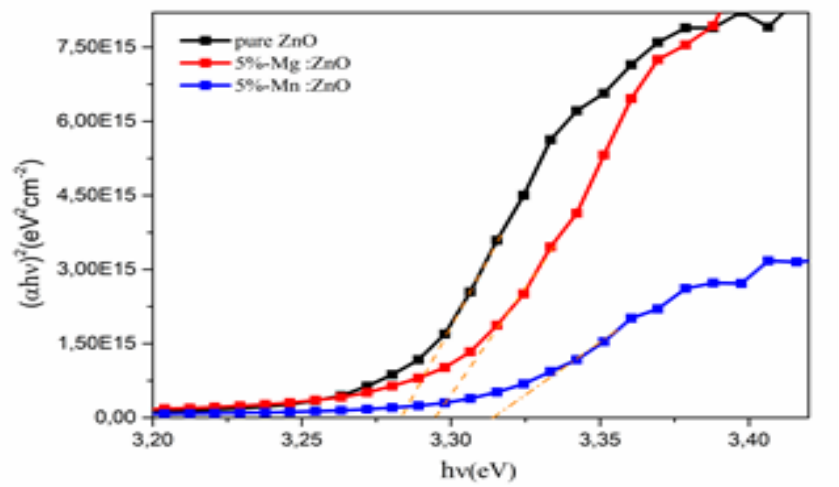

Fig. 4. Plot of (αhν)2 versus photon energy (hν) of pure ZnO, Mg-doped ZnO, and Mn-doped ZnO thin films.

4.4. Magnetic properties

To investigate the magnetic properties of all synthesized thin layers, a room-temperature vibration sample magnetometer (VSM) was used to obtain a hysteresis loop. Figure 5 represents M–H hysteresis loops for pure ZnO, Mg-doped ZnO, and Mn-doped ZnO samples measured under a magnetic field fixed at 8 KOe at room temperature. For pure ZnO samples, it can be seen that the film is magnetic in nature, and they reveal a room-temperature dominant ferromagnetic phase. It should be noted that the bulk ZnO is naturally diamagnetic or paramagnetic, and ferromagnetic behavior can be attributed to surface zinc interstitials, oxygen vacancies, and defects or impurities in the ZnO host structure. Mg-doped ZnO and Mn-doped ZnO films can show a gradual extension of the hysteresis loops compared to the undoped ZnO

sample. The coupling exchange interaction between the Mg^{2+} and Mn^{2+} ions in the zinc oxide host lattice may explain these results [24].

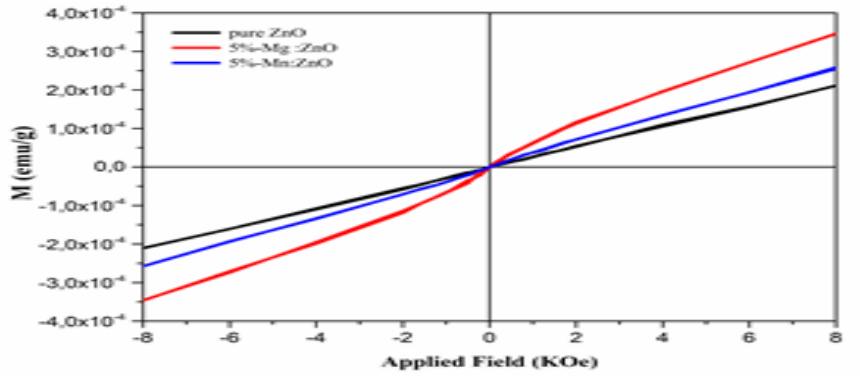

Fig. 5. The M–H hysteresis loops of pure ZnO, Mg-doped ZnO, and Mn-doped ZnO thin films.

5. Conclusion

Pure ZnO, Mg-doped ZnO, and Mn-doped ZnO nanostructured thin layers have been successfully synthesized via nebulizer spray pyrolysis (NSP) technique at 400°C on a glass substrate. The impact of substitutional doping at (5%wt) of Mg^{2+} and Mn^{2+} on the elaborated layers' structural, optical, and magnetic properties was examined. XRD results show that all prepared samples have a hexagonal wurtzite structure and polycrystalline in nature with (002) as the preferred orientation. The crystallite size increases significantly from 26.123 nm to 29.899 nm for the Mg-doped ZnO sample and then decreases to a rich 20.891 nm through the Mn-doped ZnO sample. Raman spectra demonstrate that the intensity of vibrational modes increased as doping with Mg2+ or Mn2+ ions. Optical characterization showed that the prepared samples exhibited high optical transmittance in the visible region. In addition, the band gap energy increases slightly from 3.28 to 3.31 eV as a function of doping elements. The magnetic analysis revealed that all films exhibit stable room-temperature ferromagnetism. This work shows that doping ZnO with Mn^{2+} or Mg^{2+} has potential applications in optoelectronic and DMS devices, as confirmed by optical and magnetic investigation.

References

[1] C. Buzea, I.I. Pacheco, K. Robbie, Biointerphases 2(4), MR17(2007);

[2] X.Y. Kong, Z.L. Wang, Nano Lett. 3, 1625 (2004);

[3] D. Anbuselvan, S. Nilavazhagan, A. Santhanam, N. Chidhambaram, K.V. Gunavathy, Tansir Ahamad, Saad M. Alshehri, Physica E 129, 114665(2021);

[4] Phuruangrat, T. Thongtem, S. Thongtem, Digest Journal of Nanomaterials and Biostructures 18(4), 1423(2023);

[5] S. A. H. Abbas, E. S. Hassan, O. M. Abdulmunem, Digest Journal of Nanomaterials and Biostructures 18(3), 793(2023);

[6] W. Darenfad, N. Guermat, K. Mirouh, Journal of Molecular Structure 1286, 135574(2023);

[7] B. Dey, R. Narzary, S. N. Rout, M. Kar, S. Ravi, S.K. Srivastava, Ceramics International 49(22), 35860(2023

[8] Boukhari, B. Deghfel, A. Mahroug, R. Amari, N. Selmi, S. Kheawhom, A.A. Mohamad, Ceramics International 47(12), 17276(2021);

[9] Tiwari, P.P. Sahay, Physica B: Condensed Matter 629, 413638(2022);

[10] D. N. Sree, S.P.M. Deborrah, C. Gopinathan, S.S.R. Inbanathan, Applied Surface Science 494, 116(2019);

[11] A.S. Alshammari, Z.R. Khan, M. Gandouzi, M. Mohamed, M. Bouzidi, M. Shkir, H.M. Alshammari, Optical Materials 126, 112146(2022);

[12] R.A. Mereu, A. Mesaros, T. Petrisor Jr., M. Gabor, M. Popa, L. Ciontea, T. Petrisor, Journal of Analytical and Applied Pyrolysis 104, 653(2013);

[13] N.C. Vega, B. Straube, O. Marin-Ramirez, D. Comedi, Materials Letters 333, 133684(2023

[14] V.S. Kamble, R.K. Zemase, R.H. Gupta, B.D. Aghav, S.A. Shaikh, J.M. Pawara, S.K. Patil, S.T. Salunkhe, Optical Materials 131, 112706(2022);

[15] M. Thirumoorthi, V. Ganesh, T.H. AlAbdulaal, P. Raju, S.S. Dhavud, Optical Materials 123, 111862(2022);

[16] E. Chubenko, M.W. Alhamd, V. Bondarenko, Journal of Luminescence 247, 118860(2022);

[17] F.P Jose, S.R. Achari, M.K. Jayaraj, A.A. Sukumaran, AIP Conference Proceedings 2265, 030639 (2020);

[18] Z. Ullah, M. T. Qureshi, K. Sultana, F. Ullah, A. Khalid, N. Masood, F. I.A. Abdella, S. A. Elhag, Digest Journal of Nanomaterials and Biostructures 18(3), 995(2023);

[19] N. T. Nguyen, V. A. Nguyen, Digest Journal of Nanomaterials and Biostructures 18(3), 889(2023);

[20] Gharbi, A. Boukhachem, M. Amlouk, M. Oueslati, B. Dkhil, A. Meftah, Applied Physics A 126, 604 (2020);

[21] S. Prasad, S. Bansal, S.P. Pandey, Materials Today: Proceedings 49, 3022 (2022);

[22] Q.Q. Gao, Q.X. Yu, B. Chen, H. Zhu, Journal of Alloys and Compounds 590, 446(2014);

[23] P. Dhiman, J. Chand, A. Kumar, R K Kotnala, K. M. Batoo, M Singh, Journal of alloys and compounds 578, 235(2013);

[24] Y.Q. Wang, S.L. Yuan, L. Liu, P. Li, X.X. Lan, Z.M. Tian, J.H. He, S.Y. Yin, Journal of Magnetism and Magnetic Materials 320(8), 1423(2008);